Frustration, drift, and antiphase coupling in a neural array

Oliver Weihberger* and Sonya Bahar†
Center for Neurodynamics and Department of Physics and Astronomy, University of Missouri at St. Louis, One University Boulevard, St. Louis, Missouri 63121, USA

(Received 31 August 2006; revised manuscript received 12 January 2007; published 16 July 2007)

Synchronization among neurons is critical for many processes in the nervous system, ranging from the processing of sensory information to the onset of pathological conditions such as epilepsy. Here, we study synchronization in an array of neurons, each modeled by a set of nonlinear ordinary differential equations. We find that an array of 20×20 coupled neurons undergoes a series of alternating low and high synchronization states, as measured by phase-locking and frequency entrainment, as the coupling constant is tuned. The role of long-range connections in inducing "small-world networks" has recently been of great interest in many physical and biological problems. Since long-range connections do exist in the brain, we investigated the role of such connections in our neural array. Introducing a biologically realistic percentage of long-range connections has no significant effect on synchronization. We find that it is rather the type of coupling and the total number of connections that determine the synchronization state of the array. We also show that some coupling conditions can lead to frustration in the system, resulting from an inability to simultaneously satisfy conflicting phase requirements. This frustration leads to a drift in the overall behavior of the network, which may offer an explanation for transitions between different types of neural oscillations observed experimentally.

DOI: 10.1103/PhysRevE.76.011910 PACS number(s): 87.18.Sn, 05.45.Xt, 87.19.La, 87.19.Nn

I. INTRODUCTION

The link between neural synchronization and bursting, both in experiment and in computational models, has long been of interest in various neural problems, ranging from pathological conditions such as epileptic seizures [1–4] to more subtle mechanisms of information processing in the brain [5–8]. It was recently shown [9] that a pair of neurons described by the Huber-Braun model [10], in a nearest-neighbor-coupled lattice, exhibits a series of successive synchronized and desynchronized states, passing through various bursting states as a coupling constant is tuned; increased synchronization was found to lead to increased bursting, and vice versa. In the present paper, we extend this work to investigate *global synchronization* in this model, i.e., the degree of synchronization over the *whole* array, for various types of coupling. Furthermore, since the real mammalian neocortex exhibits much more complex connectivity than a simple lattice, with a prominent feature being the existence of long-range connections, provided by the long axons of pyramidal neurons [11], we investigate the stability of synchronization patterns in the present model in response to the addition of random long-range connections. The introduction of long-range connections raises the possibility of small-world network behavior in the present model, in which rewiring of local connections in a regular network leads to a sharp drop in the effective path length between elements in the network [12]. Since small-world effects have been observed in a number of neural systems, ranging from the nematode worm *C. elegans* [12] to the human brain [13], and have been suggested to play a potential role in the dynamics of epilpetic seizure onset [14,15], we investigate the small-world properties of the present model following the addition of a biologically realistic density of long-range connections.

II. MODEL

The neural model used here is taken from Braun *et al.* [10,16], and is also described in [9]. This model, a modification of the original Hodgkin-Huxley equations for bursting neurons [17], exhibits various bursting behaviors as a single parameter T is tuned. We have chosen this model in part because it is a model of the Hodgkin-Huxley type, and therefore of a model class that is well established as realistic single-compartment models of neural activity; an additional reason for this choice of model is that one of the motivations of the present study is to extend the results in [9], which used the Huber-Braun model on the basis of its bifurcation structure and tunable bursting properties. Note also that the parameter T describes temperature in the original Huber-Braun model; here, we consider it simply as a parameter that tunes the system's bursting behavior. The membrane potential V_i for neuron i is described as

$$C_M\frac{dV_i}{dt} = -I_l - I_d - I_r - I_{sd} - I_{sr} + \xi + g\sum_j a_{ij}(V_i - V_j). \tag{1}$$

I_l is a passive leak current with

$$I_l = g_l(V_i - V_l) \tag{2}$$

and is presumed to be carried primarily by Cl^- ions; g_l is the maximum conductance and V_l is the reversal potential of the leak current. I_d and I_r are simplified depolarizing and repolarizing Hodgkin-Huxley currents, and representing the fast Na^+ and K^+ ion kinetics, respectively. I_{sd} and I_{sr} are slow subthreshold depolarizing and repolarizing currents which

*Present address: Bernstein Center for Computational Neuroscience Freiburg and Department of Neurobiology and Biophysics, University of Freiburg, D-79104 Freiburg, Germany; Electronic address: weihberger@bccn.uni-freiburg.de
†Electronic address: bahars@umsl.edu

represent Ca^{2+} and Ca^{2+}-dependent K^+ currents, respectively. They act on a slower time scale and at a subthreshold level, and their interplay results in the oscillation of the baseline membrane potential. Biologically, the Ca^{2+} current can play a significant role in the modulation of burst activity. Ca^{2+}-dependent K^+ currents are expressed in many tissues, including neurons; while their physiological role is not fully understood, their expression does appear to be altered in some human epileptic syndromes [18]. The currents are modeled as follows (for $k=d$, r, sd):

$$I_k = \rho g_k a_k (V_i - V_k), \tag{3}$$

where ρ is a scaling factor with

$$\rho = 1.3^{(T-T_0)/10},$$

g_k and V_k are the maximum conductance, and the reversal potential, of the corresponding current, respectively, and a_k is an activation variable which represents the probability of ion channel opening. It has values between 0 and 1 and is described by a differential equation:

$$\frac{da_k}{dt} = \frac{\phi(a_{k,\infty} - a_k)}{\tau_k}, \tag{4}$$

where ϕ is another temperature-dependent scaling factor with

$$\phi = 3.0^{(T-T_0)/10}.$$

Here, τ_k is a time constant and $a_{k,\infty}$ is the steady-state activation,

$$a_{k,\infty} = \frac{1}{1 + \exp[-s_k(V_i - V_{0k})]}. \tag{5}$$

The remaining subthreshold repolarizing current I_{sr} is modeled as

$$I_{sr} = \rho g_{sr} a_{sr} (V_i - V_{sr}). \tag{6}$$

Here, the activation variable has the form

$$\frac{da_{sr}}{dt} = \frac{\phi(-\eta I_{sd} - k a_{sr})}{\tau_{sr}}. \tag{7}$$

The presence of I_{sd} in this equation produces the Ca^{2+}-dependence of the K^+ current I_{sr}. The term ξ in Eq. (1) represents delta-correlated, zero-mean Gaussian white noise of variance $2D$ (where D is the noise intensity), implemented with a standard Box-Mueller algorithm as given in [19].

A coupling term c_i was introduced for each neuron i, with

$$c_i = g \sum_j a_{ij} (V_i - V_j), \tag{8}$$

where g is a coupling constant and V_i is the membrane potential of the ith neuron. $A=[a_{ij}]$ is the adjacency matrix [20], which is defined as follows. If there are n neurons, then A is an $n \times n$ matrix and the element a_{ij} is 1 if neuron i has a connection to neuron j, 0 otherwise.

Three different topological coupling schemes were used, as illustrated in Fig. 1.

Equation (8) represents the simplest possible type of coupling term, corresponding to a gap junction (direct electrotonic connection between cells, which occurs between some neurons), rather than more complex synaptic coupling. Gap junction coupling has been chosen in order to render the present model more dynamically simple; subsequent studies will address more realistic synaptic coupling. Note that the coupling term is "inhibitory," to the extent that when neuron V_j fires, neuron V_i is less likely to fire. In other words, depolarization of one neuron will cause hyperpolarization of its neighbor. Inhibitory coupling plays a major role in the dynamics of neocortical pyramidal neurons [21] as well as in the dynamics of cortical networks [22]. In addition, inhibitory connections have been implicated as playing a major role in synchronous neural firing [23].

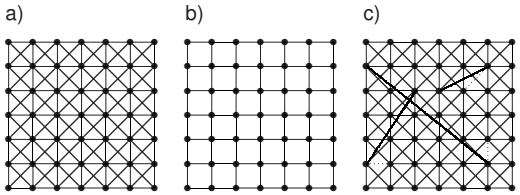

FIG. 1. (a) In the most general coupling scheme, each neuron (excluding neurons at the edges) is connected to eight nearest neighbors, including diagonals. (b) No diagonal coupling, with connections to only four nearest neighbors. (c) Array with several introduced long-range connections. Dotted lines represent broken local connections.

Table I shows the parameter values used in the model; in all cases the noise level was set at $D=0.5$, and T was set at a value of 30 °C, for which individual, uncoupled neurons all fire tonic single spikes (no bursts). We constructed a lattice of 20×20 neurons; numerical integration was performed using Euler's method, with a step size of 0.1 ms. The model has been tested with smaller step sizes, with no change observed in the results.

TABLE I. Parameter values used in the model.

Membrane capacitance $\left(\frac{\mu F}{cm^2}\right)$	$C_M=1$	
Conductances $\left(\frac{ms}{cm^2}\right)$	$g_d=1.5$	$g_{sd}=0.25$
	$g_r=2.0$	$g_{sr}=0.4$
	$g_l=0.1$	
Reversal potentials (mV)	$V_d=50$	$V_{sd}=50$
	$V_r=-90$	$V_{sr}=-90$
	$V_l=-60$	
Time constants (ms)	$\tau_d=0.1$	$\tau_{sd}=10$
	$\tau_r=2$	$\tau_{sr}=20$
Steepness (mV^{-1})	$s_d=0.25$	$s_{sd}=0.09$
	$s_r=0.25$	
Half activation (mV)	$V_{0d}=-25$	$V_{0sd}=-40$
	$V_{0r}=-25$	
Other parameters	$T=30$ °C	$T_0=25$ °C
	$\eta=0.012$	$k=0.17$
	$D=0.5$ A^2/s	

A. Analytical methods

Following the approach of Pikovsky, Rosenblum, and Kurths and others [24,25], we investigate stochastic phase synchronization, as defined by both phase-locking (in a statistical sense) *and* frequency entrainment. We used the synchronization index γ [26,27] as a basis from which to calculate a quantity $\gamma_{overall}$ as our measurement of the degree of global synchronization. We emphasize that the term global, as used here, refers to a measure of stochastic phase synchronization over the entire array, rather than to a measure of complete synchronization in the sense of Pecora and Carroll [28]. Frequency entrainment was measured by means of the standard deviation of the distribution of instantaneous frequencies. For small-world networks, we calculated the clustering coefficient C and the average path length L [12] for arrays with different percentages of introduced long-range connections. In the following, we define these quantities in detail.

1. Synchronization index $\gamma_{overall}$

We treated every neuron as a noisy 2π-periodic oscillator and assigned a discrete phase difference to a pair of neurons a and b at times t_i as

$$\phi_{ab}(t_i) = 2\pi\left(\frac{t_i - t_j}{t_{j+1} - t_j}\right), \quad t_j \leqslant t_i < t_{j+1}, \tag{9}$$

where t_i are the spike times (or burst times) of neuron a, and t_j are the spike times (or burst times) of neuron b [26,29]. A spike time was defined when the membrane potential crossed a −20 mV threshold in the positive direction. A burst time was defined as the spike time of the first spike in a burst, with a burst defined as a group of at least two successive spikes with ISIs (between the spikes comprising the burst) <90 ms. In the following, we calculate phase differences based on burst times, rather than spike times.

A phase difference measurement as given in Eq. (9) is useful for characterizing the phase relations of processes which are roughly periodic but also show stochasticity. By plotting the probability density of the phase differences and calculating the intensity of the first Fourier mode of this distribution,

$$\gamma^2 = \langle \cos\phi \rangle^2 + \langle \sin\phi \rangle^2, \tag{10}$$

where ϕ is the phase difference given in Eq. (9) and the brackets denote a time average, one obtains the synchronization index γ for any pair of neurons, which has values between 0 (no phase-locking) and 1 (perfect phase-locking).

A measurement of the *overall synchronization* of the whole array is obtained as follows. We calculated matrices $\Gamma_k = [\gamma_{ij}]_k$ containing values of γ as given in Eq. (10) where $[\gamma_{ij}]_k$ is the synchronization index for neuron (i,j) in the two-dimensional array with the kth neuron serving as a reference neuron. A quantity $\gamma_{average}(i,j)$ for a specific neuron at position (i,j) in the array is then calculated by summing the values of $\Gamma_k(i,j)$ with respect to all possible reference neurons k and dividing this sum by the number of reference neurons (in our case, a 20×20 array, this value is 400). $\gamma_{overall}$ is obtained by taking the average of all $\gamma_{average}(i,j)$'s, excluding the boundary neurons. Thus

$$\gamma_{average}(i,j) = \frac{1}{400}\sum_{k=1}^{400} \Gamma_k(i,j), \tag{11}$$

$$\gamma_{overall} = \frac{1}{18^2}\sum_{i=2}^{19}\sum_{j=2}^{19} \gamma_{average}(i,j). \tag{12}$$

Strictly speaking, $\gamma_{overall}$ measures the amount of global phase-locking, one condition for synchronization, and it perfectly served the need for one convincing measurement for global synchronization. The second condition, namely frequency entrainment, is considered in the following section.

2. Standard deviation of the frequency distribution

The instantaneous frequency

$$f = \frac{1}{t_{i+1} - t_i} \tag{13}$$

measures the inverse of the time interval between successive spike events of a single neuron. We use the term "intraburst interval" for the time period between two successive spikes within a burst and "interburst interval" for the time period between the beginning of two successive bursts. To calculate a distribution of spike intervals, one can consider all intervals between spikes, i.e., including both interburst and intraburst intervals, which leads to a frequency distribution with multiple peaks ("frequency of spikes"). Alternatively, one can consider only the interburst intervals, leading to a single-peaked frequency distribution ("frequency of bursts"). It is the latter type of distribution that we consider here. We calculate the standard deviation

$$\sigma_f = \sqrt{\langle f_n^2 \rangle - \langle f_n \rangle^2}, \tag{14}$$

where f_n is the time-averaged instantaneous frequency (of bursts) for one neuron, and the brackets denote an average over the whole array, as a measure of overall frequency entrainment in the array.

3. Small-world network characteristics

The clustering coefficient C was calculated according to [12] in the following way: every neuron v in the array has k_v neighbors (depending on its position in the array), leading to $k_v(k_v-1)$ possible connections among this neuron's neighbors. Now C_v is the ratio of the actual existing connections to all the possible ones. C is then obtained by taking the average over all C_v's. The result was normalized with respect to the clustering coefficient of a totally regular array, $C_{reg} = 0.4651$ [calculated from a regular array, as sketched in Fig. 1(a)].

The average path length L is the number of connections in the shortest connected path between two neurons, averaged over all pairs of neurons. L was obtained using the previously-described adjacency matrix A as follows. The element (i,j) of A^l is the number of different paths of length l

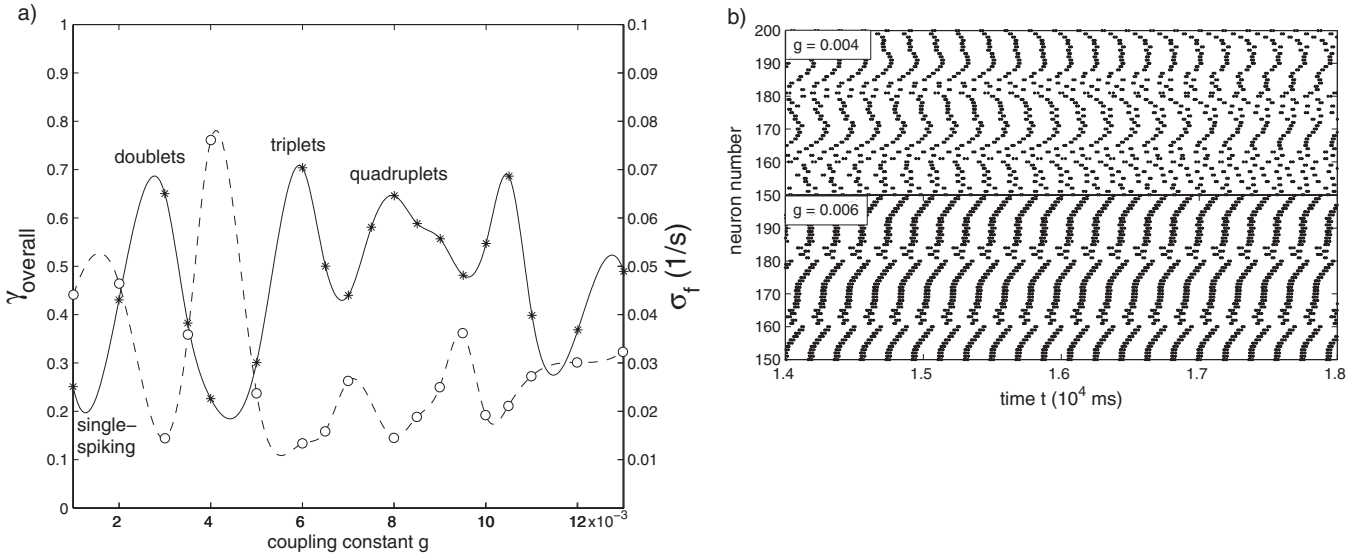

FIG. 2. (a) Alternating high and low values of $\gamma_{overall}$ (solid line, stars) and σ_f (dashed line, open circles). The spike pattern changes from doublets, to triplets, and so forth after each maximum. (b) Raster plots reveal desynchronized spiking dynamics for $g=0.004$ (top) in contrast to the more synchronized activity at $g=0.006$ (bottom). The $g=0.004$ raster plot also illustrates the phenomenon of drift, which we define as a continually changing phase relationship between neurons in the array.

from neuron i to j. With this, the average path length can easily be calculated for different topologies. The result for L was normalized with respect to the average path length of the totally regular array [Fig. 1(a)], $L_{reg}=9.3217$.

Simply speaking, C measures the "cliquishness" in the array, which is a local property, while L measures the separation between neurons, which is a global property, of the array.

III. RESULTS

A. Array with general coupling

In the case of "general coupling," illustrated in Fig. 1(a), every neuron is connected to its diagonal and nondiagonal neighbors; no long-range connections are present. We find that the whole system of 20×20 coupled neurons undergoes a series of alternating low and high synchronization index $\gamma_{overall}$ as a function of the coupling constant g, as shown in Fig. 2. At each peak value of $\gamma_{overall}$, the system takes on a different type of bursting behavior, moving from single spikes ($g=0.001$) to doublets (i.e., two-spike bursts, $g=0.003$) to triplets (i.e., three-spike bursts, $g=0.006$) and so on. The standard deviation of the frequency distribution of bursts as given in Eq. (14) is also plotted in Fig. 2.

Each value was calculated from a 20 s time series, after discarding 10 s of transients. A clear expression of frequency entrainment was observed at the same values of g where $\gamma_{overall}$ has its maxima. Note that the minima for σ_f occur at the same values of g as the maxima for $\gamma_{overall}$. Thus Fig. 2 shows that for certain values of the coupling constant, both the phase-locking and the frequency entrainment conditions are simultaneously satisfied. We observe, furthermore, oscillations in $\gamma_{overall}$, illustrating successive windows of coupling strength within which global synchronization occurs within the array. In each successive window of synchronization, the neural bursting is enhanced. This is a similar but stronger result to that in [9], where windows of phase-locking were demonstrated for only two representative neurons in the array as the coupling strength was increased. Note that the fluctuations of $\gamma_{overall}$ and σ_f remain unaltered if the amplitude of the added noise is reduced to zero (data not shown). Note also that this occurs, and indeed, our entire study is conducted, at a value of T for which, in the uncoupled case, no bursting occurs. A single uncoupled neuron will pass through various bursting regimes as T is decreased [10]. Thus the coupling could be interpreted as pushing the system along its (uncoupled) bifurcation diagram, even though the bifurcation parameter itself is held fixed. (Of course, this interpretation is metaphorical; in fact, the system is undergoing a new set of bifurcations, with the coupling constant as the bifurcation parameter.) Raster plots of spike times for two different coupling constants, shown in Fig. 2(b), illustrate the spiking behavior of a subset of the array for desynchronized (top) and synchronized (bottom) conditions.

B. Frustration results from conflicting phase requirements

According to the coupling term for two neighboring neurons i and j, $c_i \propto (V_i - V_j)$ and $c_j \propto (V_j - V_i)$, the negative sign leads to inhibition of neuron i if neuron j spikes, and vice versa. This *antiphase* coupling will tend, in principle, toward a phase difference of π between any pair of coupled neurons. Antiphase coupling in an experimental system was observed in a study of cultured human epileptic astrocytes [30], and supported by simulating the intracellular oscillations via FitzHugh-Nagumo oscillators [30]. We observe that diagonal neighbors tend much more strongly to such antiphase coupling than do nondiagonal neighbors, as shown in Fig. 3. The phase differences were calculated according to Eq. (9), with

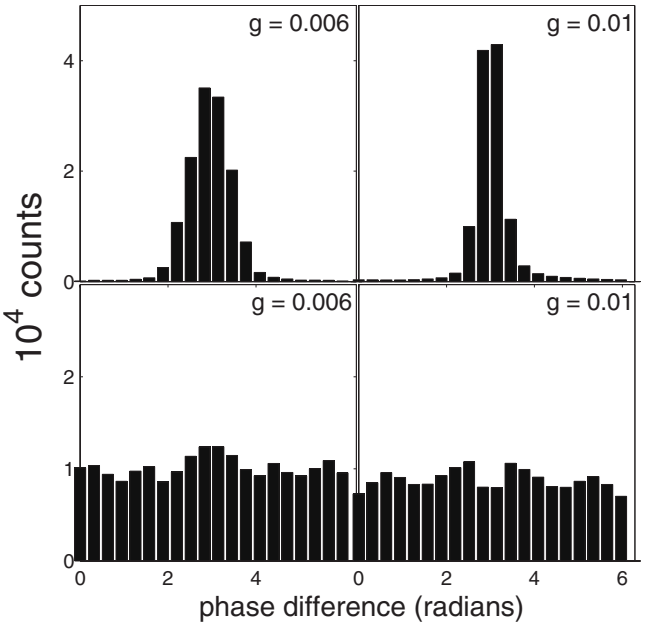

FIG. 3. Histograms of phase difference values observed between diagonally connected neurons (top row) and between nondiagonal connections (bottom row). Diagonals preferentially lock in with a phase difference of π, while nondiagonals have a flat phase difference distribution.

t_i and t_j denoting burst times for neurons a and b respectively.

The prevailing topology in the system described above, where each neuron is coupled to its eight nearest neighbors, makes it impossible to fulfill the requirement to lock in with a phase difference of π with every coupled neighbor, leading to what may be described as local *frustration* in the system. As we will see below, this frustration leads to a *drift* in the collective activity of the model system, which bears a striking resemblance to changes in field potential patterns recorded from the neocortex. By *drift*, we refer to a continuously changing phase difference between a pair or group of neurons, i.e., a situation in which a fixed phase difference is never achieved. We emphasize that frustration and drift are fundamental characteristics of the system itself. These phenomena arise in response to competing and unsatisfiable phase requirements, and the system's resulting nonstationarity, and are not simply effects of additive noise.

But why is it the diagonals who win out in the struggle to lock into antiphase coupling? The origin of the dominance of antiphase coupling between diagonal rather than nondiagonal neighbors can be understood by considering the coupling term for an arbitrary neuron i: consider a neuron i is connected to its diagonal neighbors 1,2,3,4 and to its nondiagonal neighbors a,b,c,d. The coupling term for neuron i is thus

$$c_i = g(8V_i - V_1 - V_2 - V_3 - V_4 - V_a - V_b - V_c - V_d). \quad (15)$$

The contributions of neighboring neurons (index 2*nd* for any secondary, i.e., second degree, or "once removed," neighbor of V_i) to the coupling term are thus proportional to

$$V_1 \propto g(8V_1 - V_i - V_a - V_d - 5V_{2nd}),$$

$$V_a \propto g(8V_a - V_i - V_b - V_d - V_1 - V_2 - 3V_{2nd})$$

$$\cdots.$$

Substituting this in Eq. (15) for c_i, and neglecting secondary terms, yields

$$c_i \propto g[8V_i(1+g) - 6g(V_1 + V_2 + V_3 + V_4) \cdots - 4g(V_a + V_b + V_c + V_d)]. \quad (16)$$

Thus every time one of the diagonal neighbors $(1,\ldots,4)$ spikes, the coupling term for neuron i is more significantly decreased compared to when a nondiagonal neighbor $(a,\ldots,d)$ spikes (since the coefficient of the diagonal terms is greater than that of the nondiagonal terms). Thus a spiking neuron i is more inhibited at times when its diagonal neighbors spike. So neuron i tends to lock in between two consecutive spikes of its diagonal neighbors, leading to the observed preference for antiphase coupling among diagonals.

The different locking patterns of diagonal and nondiagonal pairs can be visualized via a synchronization map. A synchronization map is a grayscale map of the synchronization index $\gamma_{overall}$ for each neuron as expressed in Eq. (11). The maps are shown in a gray scale ranging from white to black, where white indicates $\gamma_{average}(i,j)=1$, corresponding to maximal synchronization, and black indicates $\gamma_{average}(i,j)=0$, corresponding to a completely desynchronized state. The synchronization maps of Fig. 4 show a "checkerboard" pattern, which is a result of the alternating high and low values of $\gamma_{average}$ in each row and column.

C. Array with a modified coupling term

In order to investigate the effects of relaxing the frustration described above, we considered synchronization in networks with simpler topologies. A first modification was to remove the diagonal coupling, as shown in Fig. 1(b). In this system, there exists no frustration, since every connection leads to a mutual phase relationship of π as discussed further below. The graph of $\gamma_{overall}$ vs the coupling constant, shown in Fig. 5(a), has a similar shape for low coupling constants as in Fig. 2 for the general coupling case, as does the plot of the standard deviation of the frequency spectrum. A significant difference, however, is that the values of the coupling constants where extrema for $\gamma_{overall}$ and σ_f occur are higher than in the previous case. Also, for higher coupling constants ($g > 0.008$), $\gamma_{overall}$ (σ_f) remains high (low). The absence of a decrease in synchronization for high g values indicates that there is no longer any phase drift in the system. Indeed, raster plots of neural firing times show a repeating pattern of firing, with no evidence of drift in the relative phase relations between neurons, indicating that the system settles quickly to an equilibrium state of optimal firing configuration. The lack of frustration, and the consequent lack of drift, result from the fact that the system can fully comply with the requirements set up by the coupling terms.

In the case described here, nondiagonals have a preferred phase relationship of π and diagonals have a phase relation-

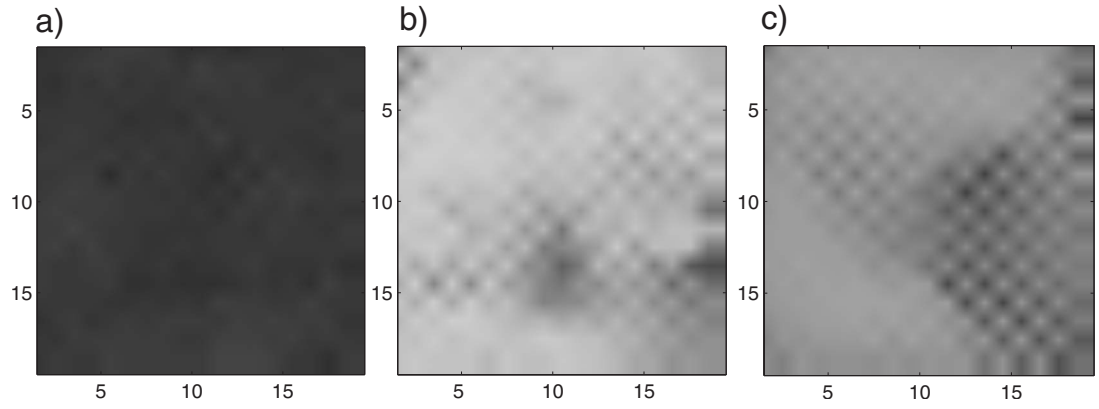

FIG. 4. Synchronization maps for (a) $g=0.004$, (b) a synchronized state at $g=0.006$, (c) $g=0.01$; the checkerboard effect increases with increasing coupling constant.

ship of 0 or 2π. The latter can be understood when one considers that diagonal neighbors are indirectly linked by two nondiagonal neighbors, each of which forces a phase difference of π. This forces the two diagonal neighbors to assume a mutual phase difference of 0 (2π). Histograms for the phase differences between diagonal and nondiagonal neighbors are shown in Fig. 5(b). In a synchronization map, the lack of frustration in the system would be evidenced by a uniform grayscale, rather than a checkerboard pattern (not shown).

D. Array with random long-range connections

Long-range connections were introduced randomly by choosing two random positions in the array (using Matlab's internal random number generator function *rand*) and coupling them via a gap junction term. The whole array solely with nearest neighbor (including diagonal) coupling has 2964 connections, so that 1% long-range connections means the introduction of 30 new long-range connections. For each newly introduced connection, one nearest-neighbor connection was removed in order to keep the number of total connections constant. Under these conditions, the system can exhibit small-world characteristics, as shown in Fig. 6(a).

C and L were calculated as a function of the percentage of long-range connections (i.e., the probability of any one connection being "rewired"). Small-world effects occur if there exists a region where $L \geqslant L_{random}$ but $C \gg C_{random}$ [12]. This means that a rapid drop of the average path length L occurs, even for a few introduced long-range connections, while the clustering coefficient remains at an almost unchanged level. Our system shows this behavior in the range of roughly 1–10 % long-range connections [the second logarithmic section on the x axis in Fig. 6(a)] which is precisely the percentage of synaptic long-range connections estimated to exist in the real mammalian cortex [11]. In this paper, we consider our gap junction model as a simplified version of a synaptically connected model, and from this perspective a comparison to the number of long range synaptic connections in the mammalian neocortex may be considered apt. However, it should be noted that recent experimental [31,32] and computational [32,33] studies of gap junction connections suggest that a similar percentage of long-range gap junctions may be active in situations of increased synchrony in the cortex.

Simulations were performed for 2, 4, 6, 8, and 10 % long-range connections; Fig. 6(b) shows $\gamma_{overall}$ as a function of g as a comparison between the general coupling case and the case with 10% introduced long-range connections. This shows that even for 10% long-range connections, the synchronization pattern still has the same alternating high and low values of $\gamma_{overall}$. (Results for 2–8 % were similar; data not shown.) Maxima occur at the same values of g as in the general coupling case, and bursting behavior remains unchanged. The path length drops precipitously, but the param-

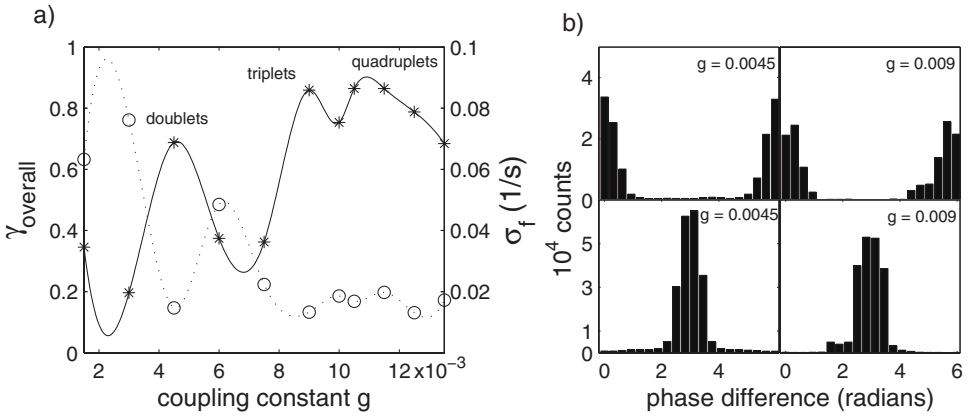

FIG. 5. (a) Alternating values for $\gamma_{overall}$ (solid line, stars) and σ_f (dashed line, circles) are observed for low coupling constants. (b) Phase difference histograms illustrating that diagonals (top row) phase-lock with a phase difference of 0 or 2π, while nondiagonals (bottom row) phase-lock with antiphase behavior due to direct coupling.

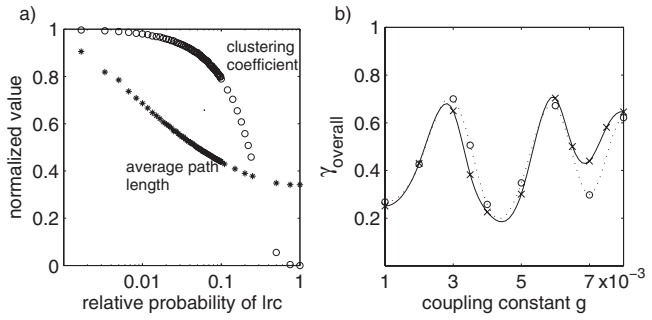

FIG. 6. (a) Average path length L (stars) and clustering coefficient C (open circles), both normalized with respect to the coefficients of a regular lattice, as a function of the probability of a given connection's being long-range. 1% long-range connections is equivalent to a probability of 0.01. (b) $\gamma_{overall}$ still alternates for 10% long-range connections (dashed line, circles). $\gamma_{overall}$ as a comparison for the general coupling case (solid line, stars).

eter dependence of synchronization and bursting regimes remains robust and unchanged.

Thus introducing a biologically realistic percentage of as much as 10% long-range connections does not have a significant effect on the overall behavior of the array, suggesting the intriguing possibility that synchronization in the neocortex may be, of evolutionary necessity, robust with respect to small variations in the percentage of long-range connections. This will be discussed further below.

E. Frustration and drift: Comparison with experiment

A simulated field potential was calculated as the collective membrane potential V for a group of neurons within the array, analogous to the field potential that would be recorded by an electrode placed in the cortex:

$$V_{field}(t) = \sum_i V_i(t). \tag{17}$$

Note that we choose to use the sum of the transmembrane potentials of all the neurons sampled, rather than the average, since the sum is more closely analogous to what a real field potential electrode measures (though, of course, a field potential records extracellular rather than intracellular potentials). The average (i.e., a mean field) could be used as well, and this obviously would not change the results other than to rescale the vertical axis in Figs. 7(b) and 7(d) below. We calculated V_{field} as a function of time for a chosen subset of the array (neurons 196-203), and observed a visible change in the appearance of the simulated field potential that correlates with an increase in drift in the raster plot. We note that the observed drift in our simulations persisted as long as the simulations continued, and thus can be attributed to the frustration in the system, rather than to dynamically transient behavior. The observed changes in the simulated field potential, namely shifts back and forth between low and high amplitude spikes, are reminiscent of the changes which have been observed in recorded field potentials during pharmacologically induced epileptic seizures in the rat neocortex

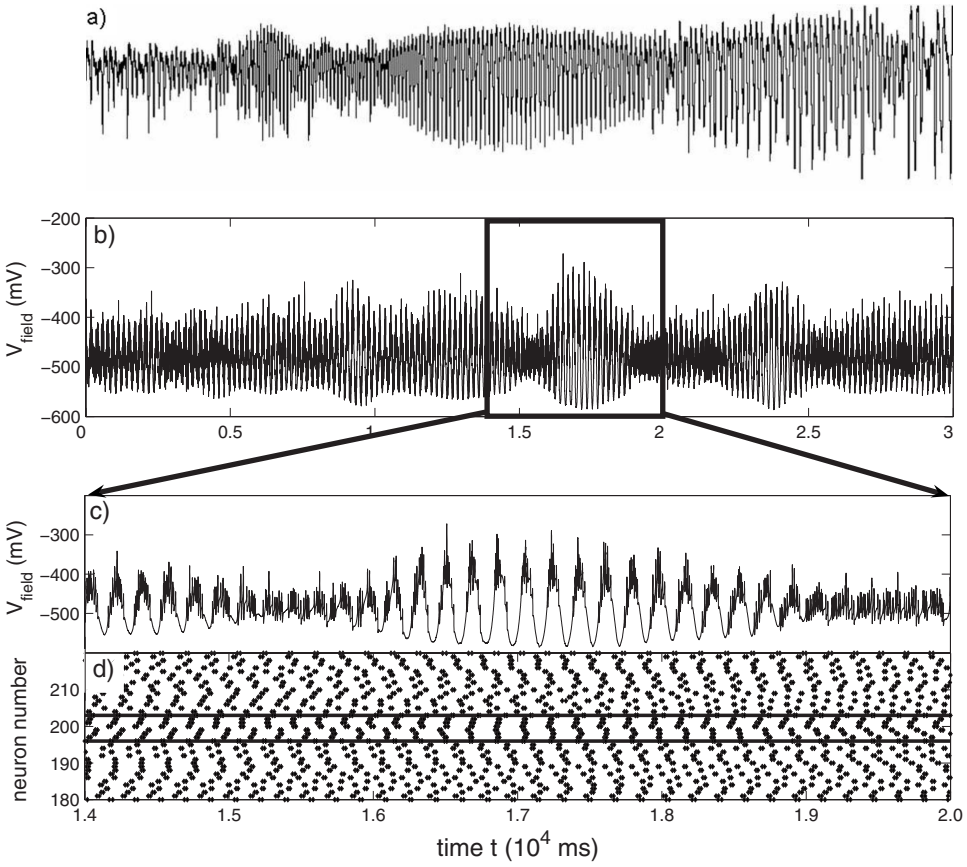

FIG. 7. (a) Field potential recording from *in vivo* rat neocortex; a focal seizure was induced by injection of 4-aminopyridine, following the method described in [34,35]. Time scale is the same as in panel (b). (b) V_{field} for an array with 10% long-range connections and $g=0.004$. V_{field} was calculated for a group of eight neurons. (c) A closer, zoomed-in, view of V_{field}. (d) Raster plot over the same time scale as panel (c), showing drift in and out of synchronization of the eight neurons (196-203, between the heavy horizontal lines) contributing to the "recorded" field potential.

[34,35], and which bear some resemblance to the transitions between spike-and-wave (SW) activity and low voltage fast activity (LVFA) observed in human seizures [36,37]. An *in vivo* field potential recording of a focal seizure in the rat neocortex, induced by the injection of 4-aminopyridine [34,35], is shown in Fig. 7(a) and a simulated field potential is shown in Fig. 7(b). A raster plot in Fig. 7(c) shows how a specific group of neurons shifts from an almost antiphase relationship to simultaneous (in-phase) spiking and back to antiphase behavior again. V_{field}, shown in Fig. 7(d), reacts accordingly, shifting from a low amplitude at $t \approx 15\,500$ ms to large-amplitude oscillations at $t \approx 17\,000$ ms and then gradually drifting back to low-amplitude oscillations as the neurons again fall out of phase. These results suggest that changes in field potential patterns in the living brain may possibly, in some circumstances, be attributable to drift of a group of neurons from one synchronization state to another; in this view, low voltage fast activity might be attributable to a preponderance of neurons firing out of phase, while a group of neurons firing in phase would lead to spike-and-wave activity. Further computational studies, including synaptic coupling, and high spatiotemporal resolution data imaging of neural activity during transitions between low voltage fast activity and spike-and-wave activity, will be required to verify this hypothesis.

IV. CONCLUSIONS

We have investigated the global synchronization properties of a coupled neural network, using a modified Hodgkin-Huxley type model for bursting neurons. We have shown that tuning the coupling strength can drive the network from a level of low synchronization to a higher one, as measured by our global synchronization parameter $\gamma_{overall}$. The previously observed finding in [9], that two individual neurons in the network show this type of behavior, has thus been generalized to the behavior of the entire array. Furthermore, we have demonstrated the same dependency on the coupling constant for frequency entrainment, which provides a second criterion for synchronization. By changing the network topology and therefore removing some frustration from the system, we show that, for large coupling constants, the system remains in a highly synchronized state, having more or less settled into an optimal configuration.

In our model, we have used gap junction coupling, thus neglecting a major component of neuronal connectivity, the synapses. We have selected gap junction coupling for the present study in order to facilitate the dynamical interpretation of the results; adding synaptic coupling terms, both excitatory and inhibitory, is an essential next step. However, we note that various studies which have investigated the effects of opened and blocked gap junctions support the idea that electrotonic coupling is fundamentally involved in the expression of ictal (seizure) discharges and in the control of duration and propagation of epileptic seizures *in vivo* [38,39]. It has been suggested by Traub [40] that gap junctions may be the main contributor to very fast oscillations leading to epileptiform bursts.

We find that randomly introduced long-range connections have no effect on the system's synchronizability, for percentages of long-range connections similar to those found in the mammalian neocortex. Furthermore, the fluctuations of regimes of high and low synchronization, as the coupling constant is tuned, remain unchanged compared to the case with only local connections. This suggests the hypothesis that brain's response may be robust with respect to small changes in topology. A similar conclusion was suggested by Percha *et al.* [14].

However, such evolutionary hypotheses about the robustness of brain topology must be approached with caution. Some models have been studied in which a small percentage of rewirings, within the small-world regime, do significantly affect network behavior. For example, a network of coupled Hodgkin-Huxley neurons were shown to have a fast response of coherent oscillations to an input stimulus under small-world conditions, with about 5% long-range connections [41]. These oscillations occurred with much lower amplitude when the network was connected as simply a regular lattice, and became incoherent when the network was entirely randomly connected. Such studies emphasize the critical need for more experimental studies on the effects of neural connectivity both in small *in vitro* networks, and *in vivo*, in order to identify the actual physiological role(s) of long-range connections in the network dynamics of real neural tissue.

Interestingly, Percha *et al.* also demonstrated that, in a network of coupled Hindmarsh-Rose neurons, rewiring probabilities in the range of 0.3–0.4, corresponding to 30–40 % of long-range connections, can drive the network, for a fixed coupling constant, from a previously disordered temporal state to a globally ordered one [14]. This percentage of long-range connections may be unrealistic with regard to the healthy mammalian neocortex, and therefore it was suggested that this situation may correspond to a pathological (epileptic) rather than normal regime: the authors drew an analogy between an increased number of long-range connections and the axonal sprouting observed in hippocampal tissue from rats with kainate-induced epilepsy [14]. Another study on models of modular networks has shown that random long-range coupling among modules could enhance the synchronizability of the studied system [42]. In these studies, a transition phenomenon was uncovered in which the network's synchronizability exhibits different behaviors, depending on a parameter that controls the probability of having random long-range links in the network. The effect of high percentages of long-range connections have yet to be fully investigated in our model; we note that such percentages, however, would lie outside the small-world regime in our system [Fig. 6(a)].

Finally, we address the phenomenon of gradual drift in the relative synchronization within a neural population. Interestingly, stationary but persistently "erratic" behavior has recently been noted in a network of leaky integrate-and-fire neurons with inhibitory connections, suggesting that drift phenomena may be prevalent in various types of neural models [43]. We suggest that, in our case, drift is a result of local frustration and each neuron's inability to simultaneously satisfy all the phase-locking demands of its neighbors; negligible drift was observed in the "frustration-free" array with a modified coupling term, in which all local phase-locking demands could be satisfied. We suggest that such drift might

contribute to observed changes in field potential oscillations during epileptic seizures.

ACKNOWLEDGMENTS

O.W. gratefully thanks the Landesstiftung Baden-Württemberg for financial support. S.B. gratefully acknowledges support from startup funds provided by the University of Missouri at St. Louis, and from an NSF CAREER grant (Grant No. PHY-0547647). The data shown in Fig. 7(a) were recorded by S.B. while working in the laboratory of Theodore H. Schwartz, M.D., in the Department of Neurological Surgery at Weill-Cornell Medical College of Cornell University, supported by NIH/NINDS Grant No. R21 NS044812 (to T.H.S.). The authors thank Professor Frank Moss and Dr. Jorge Brea for many useful discussions.

[1] R. D. Traub and R. K. Wong, Neuroscience (Oxford) **6**, 223 (1981).
[2] F. E. Dudek, R. W. Snow, and C. P. Taylor, Adv. Neurol. **44**, 593 (1986).
[3] R. K. S. Wong, R. D. Traub, and R. Miles, *Advances in Neurology* (Raven Press, New York, 1986).
[4] M. S. Jensen and Y. Yaari, J. Neurophysiol. **77**, 1224 (1997).
[5] A. Wrobel, Acta Neurobiol. Exp. (Warsz) **60**, 247 (2000).
[6] P. Fries, J. H. Reynolds, A. E. Rorie, and R. Desimone, Science **291**, 1560 (2001).
[7] E. Niebur, S. S. Hsiao, and K. O. Johnson, Curr. Opin. Neurobiol. **12**, 190 (2002).
[8] J. Fell, G. Fernandez, P. Klaver, C. E. Elger, and P. Fries, Brain Res. Rev. **42**, 265 (2003).
[9] S. Bahar, Fluct. Noise Lett. **4**, 287 (2004).
[10] H. A. Braun, M. T. Huber, M. Dewald, K. Schäfer, and K. Voigt, Int. J. Bifurcation Chaos Appl. Sci. Eng. **8**, 881 (1998).
[11] V. Braitenberg and A. Schüz, *Cortex: Statistics and Geometry of Neuronal Connectivity* (Springer, New York, 1998).
[12] D. J. Watts and S. H. Strogatz, Nature (London) **393**, 440 (1998).
[13] V. M. Eguíluz, D. R. Chialvo, G. A. Cecchi, M. Baliki, and A. V. Apkarian, Phys. Rev. Lett. **94**, 018102 (2005).
[14] B. Percha, R. Dzakpasu, M. Zochowski, and J. Parent, Phys. Rev. E **72**, 031909 (2005).
[15] T. I. Netoff, R. Clewley, S. Arno, T. Keck, and J. A. White, J. Neurosci. **24**, 8075 (2004).
[16] W. Braun, B. Eckhardt, H. A. Braun, and M. T. Huber, Phys. Rev. E **62**, 6352 (2000).
[17] A. L. Hodgkin and A. F. Huxley, J. Physiol. (London) **117**, 500 (1952).
[18] W. Du, J. F. Bautista, H. Yang, A. Diez-Sampedro, S. A. You, L. Wang, P. Kotagal, H. O. Luders, J. Shi, J. Cui, G. B. Richerson, and Q. K. Wang, Nat. Genet. **37**, 733 (2005).
[19] R. F. Fox, I. R. Gatland, R. Roy, and G. Vemuri, Phys. Rev. A **38**, 5938 (1988).
[20] F. Buckley and F. Harray, *Distance in Graphs* (Addison-Wesley, Redwood City, CA, 1990).
[21] A. Destexhe, M. Rudolph, J.-M. Fellous, and T. J. Sejnowski, Neuroscience (Oxford) **107**, 13 (2001).
[22] N. Brunel and X. J. Wang, J. Comput. Neurosci. **11**, 63 (2003).
[23] C. van Vreeswijk, L. F. Abbott, and G. B. Ermentrout, J. Comput. Neurosci. **1**, 313 (1994).
[24] A. Pikovsky, M. Rosenblum, and J. Kurths, *Synchronization: A Universal Concept in Nonlinear Sciences* (Cambridge University Press, Cambridge, England, 2003).
[25] M. G. Rosenblum, A. S. Pikovsky, and J. Kurths, Phys. Rev. Lett. **76**, 1804 (1996).
[26] S. Bahar and F. Moss, Int. J. Bifurcation Chaos Appl. Sci. Eng. **13**, 2013 (2003).
[27] M. Rosenblum, A. Pikovsky, C. Schäfer, P. A. Tass, and J. Kurths, in *Handbook of Biological Physics 4: Neuro-Informatics and Neural Modelling*, edited by F. Moss and S. Gielen (Elsevier Science, Oxford, 2000), Chap. 9, p. 279–322.
[28] L. M. Pecora and T. L. Carroll, Phys. Rev. Lett. **64**, 821 (1990).
[29] A. Neiman, X. Pei, D. Russell, W. Wojtenek, L. Wilkens, F. Moss, H. A. Braun, M. T. Huber, and K. Voigt, Phys. Rev. Lett. **82**, 660 (1999).
[30] G. Balázsi, A. Cornell-Bell, A. B. Neiman, and F. Moss, Phys. Rev. E **64**, 041912 (2001).
[31] T. Fukuda, T. Kosaka, W. Singer, and R. A. W. Galuske, J. Neurosci. **26**, 3434 (2006).
[32] R. D. Traub, N. Kopell, A. Bibbig, E. H. Buhl, F. E. N. LeBeau, and M. A. Whittington, J. Neurosci. **21**, 9478 (2001).
[33] F. Saraga, L. Ng, and F. K. Skinner, J. Neurophysiol. **95**, 1669 (2006).
[34] S. Bahar, M. Suh, M. Zhao, and T. H. Schwartz, NeuroReport **17**, 499 (2006).
[35] S. Bahar, M. Suh, A. Mehta, and T. H. Schwartz, in *Bioimaging in Neurodegeneration*, edited by P. A. Broderick, D. N. Rahni, and E. H. Kolodny (Humana Press, Totowa, NJ, 2005), Chap. 14, p. 149–175.
[36] R. L. Kutsy, D. F. Farrell, and G. A. Ojemann, Epilepsia **30**, 257 (1999).
[37] S. Lee, D. D. Spencer, and S. S. Spencer, Epilepsia **41**, 297 (2000).
[38] R. Köhling, S. J. Gladwell, E. Bracci, M. Vreugdenhil, and J. G. Jefferys, Neuroscience (Oxford) **105**, 597 (2001).
[39] Z. Gajda, E. Gyengesi, E. Hermesz, K. Salid, and M. Szente, Epilepsia **44**, 1596 (2003).
[40] R. D. Traub, M. A. Whittington, E. H. Buhl, F. E. N. LeBeau, A. Bibbig, S. Boyd, H. Cross, and T. Baldeweg, Epilepsia **42**, 153 (2001).
[41] L. F. Lago-Fernández, R. Huerta, F. Corbacho, and J. A. Sigüenza, Phys. Rev. Lett. **84**, 2758 (2000).
[42] K. Park, Y. Lai, S. Gupte, and J. Kim, Chaos **16**, 015105 (2006).
[43] R. Zillmer, R. Livi, A. Politi, and A. Torcini, Phys. Rev. E **74**, 036203 (2006).